

Improved flux-surface parameterization through constrained nonlinear optimization

Citation for published version (APA):

JET Contributors, Snoep, G., Koenders, J. T. W., & Citrin, J. (2023). Improved flux-surface parameterization through constrained nonlinear optimization. *Physics of Plasmas*, 30(6), Article 063906.
<https://doi.org/10.1063/5.0145001>

Document license:
CC BY

DOI:
[10.1063/5.0145001](https://doi.org/10.1063/5.0145001)

Document status and date:
Published: 01/06/2023

Document Version:
Publisher's PDF, also known as Version of Record (includes final page, issue and volume numbers)

Please check the document version of this publication:

- A submitted manuscript is the version of the article upon submission and before peer-review. There can be important differences between the submitted version and the official published version of record. People interested in the research are advised to contact the author for the final version of the publication, or visit the DOI to the publisher's website.
- The final author version and the galley proof are versions of the publication after peer review.
- The final published version features the final layout of the paper including the volume, issue and page numbers.

[Link to publication](#)

General rights

Copyright and moral rights for the publications made accessible in the public portal are retained by the authors and/or other copyright owners and it is a condition of accessing publications that users recognise and abide by the legal requirements associated with these rights.

- Users may download and print one copy of any publication from the public portal for the purpose of private study or research.
- You may not further distribute the material or use it for any profit-making activity or commercial gain
- You may freely distribute the URL identifying the publication in the public portal.

If the publication is distributed under the terms of Article 25fa of the Dutch Copyright Act, indicated by the "Taverne" license above, please follow below link for the End User Agreement:

www.tue.nl/taverne

Take down policy





If you believe that this document breaches copyright please contact us at:

openaccess@tue.nl

providing details and we will investigate your claim.

RESEARCH ARTICLE | JUNE 14 2023

Improved flux-surface parameterization through constrained nonlinear optimization

G. Snoep ; J. T. W. Koenders ; C. Bourdelle ; J. Citrin ; JET Contributors



Physics of Plasmas 30, 063906 (2023)

<https://doi.org/10.1063/5.0145001>

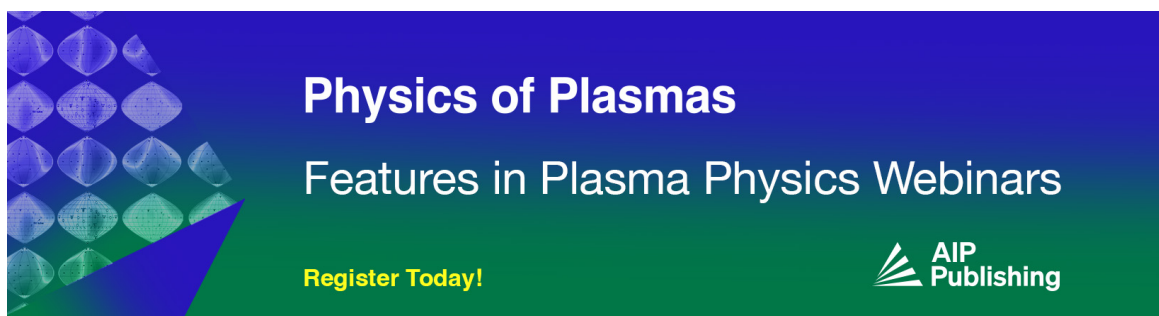


View
Online




Export
Citation

CrossMark



Physics of Plasmas
Features in Plasma Physics Webinars

Register Today!



Improved flux-surface parameterization through constrained nonlinear optimization

Cite as: Phys. Plasmas **30**, 063906 (2023); doi: [10.1063/5.0145001](https://doi.org/10.1063/5.0145001)

Submitted: 2 February 2023 · Accepted: 25 May 2023 ·

Published Online: 14 June 2023



View Online



Export Citation



CrossMark

G. Snoep,^{1,2,a)} J. T. W. Koenders,^{1,3} C. Bourdelle,⁴ J. Citrin,^{1,2} and JET Contributors^{b)}

AFFILIATIONS

¹DIFFER - Dutch Institute for Fundamental Energy Research, 5612 AJ Eindhoven, Netherlands

²Department of Applied Physics and Science Education, Eindhoven University of Technology, 5612 AJ Eindhoven, Netherlands

³Department of Mechanical Engineering, Control Systems Technology Group, Eindhoven University of Technology, 5612 AJ Eindhoven, Netherlands

⁴CEA (Commissariat à l'Energie Atomique), IRFM, 13108 Saint-Paul-lez-Durance, France

^{a)} Author to whom correspondence should be addressed: g.snoep@diffier.nl

^{b)} See author list of J. Mailloux *et al.*, Nucl. Fusion **62**, 042026 (2022).

ABSTRACT

Parameterization of magnetic flux-surfaces is often used for magnetohydrodynamic stability analysis and microturbulence modeling in tokamaks. Shape parameters for such local parameterization of a (numerical) equilibrium are traditionally computed analytically using geometrically derived quantities. However, often the shape is approximated by the average of values for different sections of the flux-surface contour or a truncated series, which does not guarantee an optimal fit. Here, instead nonlinear least squares optimization is used to compute these parameters, with a weighted sum of squared error cost function that is robust to outliers. This method results in a lower total absolute error for both the parameterization of the flux-surface contour and the poloidal magnetic field density than current methods for several parameterizations based on the well-known “Miller geometry.” Furthermore, rapid convergence of shape parameters is achieved, no approximate geometric measurements of the contour are needed, and the method is applicable to any analytical shape parameterization. Validation with local, linear gyrokinetic simulations using these optimized shape parameters showed reduced root mean square errors in both the growth rate and frequency spectra when compared with simulations based on numerical equilibria. In particular, the popular Turnbull–Miller parameterization benefits from this approach, extending its usability closer toward the last-closed flux-surface for cases with minor up-down asymmetry.

© 2023 Author(s). All article content, except where otherwise noted, is licensed under a Creative Commons Attribution (CC BY) license (<http://creativecommons.org/licenses/by/4.0/>). <https://doi.org/10.1063/5.0145001>

I. INTRODUCTION

The magnetic field in a tokamak self-organizes into nested, axisymmetric surfaces of constant magnetic pressure, so-called flux-surfaces. Radial transport in tokamak plasmas originates mostly from instabilities that are aligned with the field on these surfaces. This is often exploited in the choice of coordinate system for transport simulations to speed up calculations; hence, a local description of the magnetic equilibrium suffices.

Mercier and Luc originally developed the *local equilibrium method* in the context of MHD stability analysis,¹ but it has since also been widely adopted in neoclassical and microturbulence tokamak transport calculations. As highlighted by Miller *et al.*,² the information required to solve the Grad–Shafranov equation using the local equilibrium method consists of (1) the flux-surface shape; (2) the poloidal magnetic field component along the flux-surface; and (3) the components of the

toroidal current p' and ff' , which, in practice, are computed from the local safety factor q , magnetic shear \hat{s} , and normalized pressure gradient α . Although this information can be extracted from numerically generated equilibria, as done routinely these days, this requires recomputation of the equilibrium for every change in magnetic geometry. For increased flexibility in exploring the impact of various geometry changes (and historically because of limited computational power), a number of approximate analytical flux-surface parameterizations have been developed.^{2–8} The most popular of these is the so-called Miller geometry, often used interchangeably to refer to both the original parameterization² and its extension by Turnbull *et al.* with elevation and squareness⁵ (recently referred to as Turnbull–Miller⁸). Even though its inherent up-down symmetric flux-surface shape limits its accuracy, e.g., near the separatrix, it has been ubiquitous in microturbulence cross-code validation studies in the plasma core.^{9–11}

Both Miller *et al.*² and subsequently Luce⁷ presented analytical, geometry-based methods of calculating shape parameters from a reference flux-surface contour. In practice, this contour is typically traced on a rectangular grid of the poloidal magnetic flux that has a limited resolution. This means that the required measurements of, e.g., the flux-surface extrema have to be approximated through interpolation or in some other manner. Another source of approximation is the fact that tokamak plasmas are generally not up-down symmetric in the poloidal plane, e.g., due to shaping near the plasma boundary for exhaust purposes. Thus, measurements of flux-surface extrema with respect to its centroid can also differ along its contour, leading to multiple values for the shape parameters depending on which extrema of the plasma are used. The definition of plasma shape by Luce,⁷ which has since become the standard in the IMAS data dictionary,¹² solves this by allowing for piece-wise parameterization. However, the parameterized local equilibrium models used in microturbulence codes allow only a single value for the shape parameters as input in lieu of the numerical challenges of implementing all quantities and equations in piece-wise fashion. Therefore, often the averages of the different values for different sections of the flux-surface contour are taken as approximate inputs. This can lead to discrepancies between microturbulence predictions simulated with parameterized and exact numerical geometry in regions of the plasma that are strongly shaped, e.g., L-mode near-edge or the pedestal region in H-mode. Although more general parameterizations that mitigate this exist, e.g., Candy's general Fourier expansion⁶ and the Miller eXtended Harmonic (MXH) formulation by Arbon *et al.*,⁸ these are not (yet) utilized widely. Until then, as full-plasma radius integrated transport modeling with TGLF,^{13,14} a quasi-linear turbulent transport model with Turnbull–Miller parameterization of the local equilibrium, becomes more commonplace,^{15,16} accurate shape parameters in these regions are needed.

The method presented here avoids the need for approximations by using bounded nonlinear least squares optimization to compute the shape parameters that match the reference flux-surface contour best. As a demonstration, we apply this methodology to the aforementioned Turnbull–Miller parameterization. Numerical equilibria of two JET-ILW discharges with slightly different plasma shapes are used to illustrate the benefits of this approach. We then validate the method by comparing local, linear gyrokinetic simulations with the GENE code¹⁷ that use parameterized local equilibrium, with both the averaged

analytic and optimized shape parameters, against such simulations that use a numerical equilibrium. To show that this method generalizes to asymmetric shapes and parameterizations, we then apply it to the aforementioned Fourier and MXH parameterizations.

This paper is structured as follows. A summary of the Turnbull–Miller parameterization is provided in Sec. II, followed by a detailed description of the optimization routine in Sec. III. The two JET-ILW discharges used to demonstrate the routine are introduced in Sec. IV to examine the accuracy and convergence properties of the optimization. This is followed by linear gyrokinetic validation using these discharges in Sec. V. Asymmetry and the generalizability of the method are discussed in Sec. VI. Finally, the conclusions and discussion follow in Sec. VII.

II. TURNBULL–MILLER PARAMETERIZATION

The Turnbull–Miller flux-surface parameterization⁵ is given by

$$\begin{aligned} R_s &= R_0 + r \cos(\theta + \arcsin \delta \sin \theta), \\ Z_s &= Z_0 + r\kappa \sin(\theta + \zeta \sin 2\theta), \end{aligned} \quad (1)$$

where R_0 is the plasma major radius, Z_0 is the average plasma elevation, r is the plasma minor radius, κ , δ , and ζ are the plasma elongation, triangularity, and squareness, respectively, and $\theta \in [0, 2\pi]$ is the poloidal angle. κ , δ , and ζ all have up-down symmetric shaping effects due to being in phase with (an integer fraction of) the poloidal angle θ . Thus, for this parameterization of a flux-surface, a set of six shape parameters is required,

$$\mathbf{x} = \{R_0, Z_0, r, \kappa, \delta, \zeta\}, \quad (2)$$

with generalized bounds $\mathbf{l} = \{0, -\infty, 0, 0, -1, -\frac{1}{2}\}$ and $\mathbf{u} = \{\infty, \infty, \infty, 1, \frac{1}{2}\}$. In practice, these bounds can be reduced to device-specific limits.

The poloidal magnetic field along the flux-surface is given by²

$$B_p = |\nabla \phi \times \nabla \psi| = \frac{\partial_r \psi}{R_s} |\nabla r|, \quad (3)$$

where ϕ is the toroidal angle, and ψ is the poloidal flux. Using Mercier–Luc coordinates to calculate $|\nabla r|$ and some algebra,^{2,6} we obtain

$$B_p = \frac{\partial_r \psi R_s^{-1} \sqrt{c_\delta^2 + \kappa^2 c_\zeta^2}}{c_\zeta \kappa [\partial_r R_0 + \cos(\theta_R) - s_\delta \sin \theta \sin \theta_R] + c_\delta [\partial_r Z_0 + \kappa((s_\kappa + 1) \sin(\theta_Z) + s_\zeta \sin(2\theta) \cos(\theta_Z))]}, \quad (4)$$

where

$$c_\delta \doteq \sin(\theta_R)(1 + \arcsin(\delta) \cos \theta), \quad (5)$$

$$c_\zeta \doteq \cos(\theta_Z)(1 + 2\zeta \cos(2\theta)), \quad (6)$$

$$\theta_R \doteq \theta + \arcsin(\delta) \sin \theta, \quad (7)$$

$$\theta_Z \doteq \theta + \zeta \sin(2\theta), \quad (8)$$

$$s_\kappa \doteq \frac{r \partial_r \kappa}{\kappa}, \quad (9)$$

$$s_\delta \doteq \frac{r \partial_r \delta}{\sqrt{1 - \delta^2}}, \quad (10)$$

$$s_\zeta \doteq r \partial_r \zeta. \quad (11)$$

Equation (4) involves derivatives of shape parameters with respect to the plasma minor radius r . Therefore, a set of five additional shape-derivative parameters,

$$\hat{\mathbf{x}} = \{\partial_r R_0, \partial_r Z_0, s_\kappa, s_\delta, s_\zeta\}, \quad (12)$$

with the generalized bounds $\hat{l} = \{-\infty\}^5$ and $\hat{u} = \{\infty\}^5$, is required to complete the parameterization of the local equilibrium. The inclusion of flux-surface elevation Z_0 and its radial derivative $\partial_r Z_0$ does allow for up-down asymmetry of B_p , but this is typically relatively minor.

The toroidal magnetic field along the flux-surface is given by

$$B_t = \frac{f_p(\psi)}{R_s}, \quad (13)$$

where f_p is the poloidal current function.

III. OPTIMIZATION ROUTINE

In this section, the implementation of the shape parameter optimization routine is explained. As a starting point, a numerical Grad–Shafranov equilibrium solution, resulting in a poloidal flux map $\psi(R, Z)$ on a rectangular R, Z grid, is assumed. To compute shape parameters that best match a reference flux-surface at a radial location r from the magnetic axis, such that $\psi(r) = \psi_{\text{ref}}$, the following methodology is used:

- **Trace flux-surface:** The closed contour $\{R_r(\theta_r), Z_r(\theta_r) \mid \theta_r \in [0, 2\pi], \psi(R_r, Z_r) = \psi_{\text{ref}}\}$ is traced. The contour tracing algorithm developed for this only considers grid lines in a bounding box $\{R_{\text{bb}}, Z_{\text{bb}} \mid \psi(R_{\text{bb}}, Z_{\text{bb}}) = \psi_{\text{lcs}}\}$ centered at the magnetic axis, where ψ_{lcs} is the poloidal flux at the last-closed flux-surface (LCFS) contour.
- **Compute analytic shape parameters:** The average analytic $R_0, Z_0, r, \kappa, \delta,$ and ζ are computed for the reference flux-surface using the definitions in Miller *et al.*² and Luce.⁷ Flux-surface extrema coordinates required for this are approximated by computing the position, where the derivative of a fifth-order polynomial fit to a limited number of poloidal points is equal to zero.
- **Optimize R_s, Z_s fit:** Shape parameters that best match the reference flux-surface are calculated with nonlinear least squares. A robust least squares solver, as implemented in the open-source Python package `scipy.optimize`,¹⁸ is used for this. Among the available options in this package, the utilized implementation is based on a “trust region interior reflective” (TIR) algorithm¹⁹ to minimize a bound-constrained, weighted sum of squared error cost function,

$$\mathbf{x} = \min_{\mathbf{x} \in \mathbb{R}^n} \left\{ \frac{1}{2} \sum_{i=0}^{N_\theta-1} \rho(f_i(\mathbf{x})^2) : \mathbf{l} \leq \mathbf{x} \leq \mathbf{u} \right\}, \quad (14)$$

where N_θ is the total number of poloidal points θ_i of the reference flux-surface contour, $\rho(s)$ is the residual function, $f_i(\mathbf{x})$ is the residual, and \mathbf{l} and \mathbf{u} are the lower and upper bounds for \mathbf{x} . Averaged analytical shape parameters are used as the initial condition. The `soft_l1` residual function,¹⁸

$$\rho(s) = 2(\sqrt{|1+s|} - 1), \quad (15)$$

is used to make the minimization problem robust to outliers.²⁰ This is similar to the Huber loss,²¹ a nonlinear, smooth approximation to the ℓ_1 loss. We calculate the residual as the weighted sum of ℓ_1 and ℓ_2 ,

$$f_i(\mathbf{x}) = N_\theta(\ell_1(\mathbf{x}, \theta_i) + \ell_2(\mathbf{x}, \theta_i)), \quad (16)$$

where ℓ_1 and ℓ_2 are the two-dimensional Manhattan and Euclidian distances between parameterized and reference coordinates of the flux-surface contour, respectively. The sum of the distances was found to perform better than using either in isolation, as it combines the speed of using the ℓ_1 norm, with the accuracy of using the ℓ_2 norm.²²

Due to the Turnbull–Miller parameterization involving poloidal modifications in both R_s and Z_s , the parameterization θ -grid cannot be calculated directly from the reference θ_r -grid. Therefore, to compute ℓ_1 and ℓ_2 , each iteration of the least squares, the reference flux-surface is resampled by interpolating the discrete data on the basis of the effective poloidal angle of the parameterization,

$$\theta_s = \arctan\left(\frac{Z_s - Z_0}{R_s - R_0}\right), \quad (17)$$

where the result of the arctan is shifted such that $\theta_s \in [0, 2\pi]$. For parameterizations where a direct relation between θ and θ_r exists,⁸ this step is not required.

- **Solve $\hat{\mathbf{x}}$:** The set of shape-derivative quantities can be computed in two ways: (1) self-consistently, by taking the radial derivative of \mathbf{x} for several closely spaced consecutive flux-surfaces or (2) consider the set additional degrees of freedom also to be optimized with a least squares (see Appendix A for more details). Only the first option is considered here.

This routine has been implemented in a new open-source Python package called MEGPy,²³ which can be both called as a stand-alone tool and integrated in other workflows. It currently includes the Miller,² Turnbull–Miller,⁵ general Fourier expansion by Candy⁶ (both the original and the GENE implementation), and MXH by Arbon *et al.*⁸ flux-surface parameterizations, and others can easily be added.

IV. ACCURACY AND CONVERGENCE

Numerical equilibria from the L-mode phase of neutral beam injection (NBI) heated deuterium JET-ILW discharges #83164 and #95473 are used to demonstrate the optimization routine. See Table I for their typical optimized shape and plasma parameters. These two discharges were selected because they have slightly differing plasma shapes with limited up-down asymmetry, while their discharge scenarios and line-averaged plasma densities were similar, see Vincenzi *et al.*²⁴ for more details. The H-mode power thresholds of these discharges also differ significantly. While a detailed analysis of this is outside of the scope of this paper, this represents a pertinent example where investigating the impact of their shaping on the turbulent transport with the use of well-fitted parameterized local equilibria is of interest.

To generate numerical equilibria, the fixed-boundary Grad–Shafranov solver ESCO²⁵ was used. The last-closed flux-surfaces from previous pressure-constrained, free-boundary EFIT++^{26,27} equilibrium calculations were used as boundary in ESCO. ESCO was run coupled to the JETTO transport solver²⁵ in current diffusion simulations until the normalized toroidal flux coordinate ρ_{tor} where $q=1$ matched the approximate radial position of the sawtooth inversion-radius ρ_{inv} , as determined from electron cyclotron emission (ECE) measurements. Plasma profiles used in JETTO came from Gaussian process regression fits²⁸ to experimental measurements, time-averaged

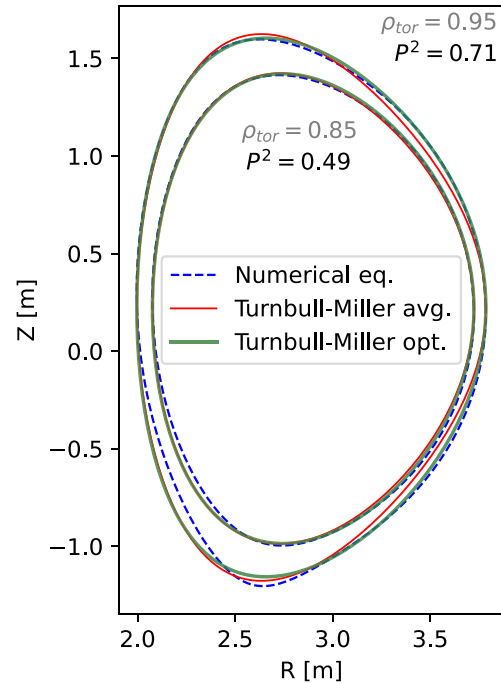
TABLE I. Overview of discharge specific input values for linear local gyrokinetic simulations with GENE for JET-ILW discharges #83164 and #95473 for $\rho_{\text{tor}} = 0.85$ and $\rho_{\text{tor}} = 0.95$. R_0 , Z_0 , and r are in meters, n_e in 10^{19} m^{-3} , and T in keV, and the rest of the values are dimensionless. Shape parameters were optimized with $N_\theta = 7200$.

Shot	#83164		#95473	
	0.85	0.95	0.85	0.95
R_0	2.900	2.891	2.890	2.878
Z_0	0.218	0.224	0.245	0.246
r	0.824	0.894	0.839	0.913
κ	1.461	1.543	1.432	1.495
δ	0.190	0.261	0.129	0.171
ζ	-0.016	-0.019	-0.018	-0.021
$\partial_r R_0$	-0.123	-0.137	-0.144	-0.171
$\partial_r Z_0$	0.092	0.020	0.056	-0.100
s_κ	0.492	0.948	0.396	0.681
s_δ	0.711	1.050	0.367	0.718
s_ζ	0.035	-0.201	-0.002	-0.128
q	2.616	3.645	2.910	3.917
\hat{s}	3.004	5.978	2.756	5.092
α	0.129	0.193	0.122	0.362
n_e	1.485	1.091	1.465	0.995
T_e	0.555	0.221	0.640	0.296
T_i/T_e	1.056	1.685	0.942	1.213
R_0/L_{m_e}	8.139	18.648	5.410	37.872
R_0/L_{T_e}	24.349	56.144	19.503	47.797
R_0/L_{T_i}	14.574	23.573	7.364	48.720

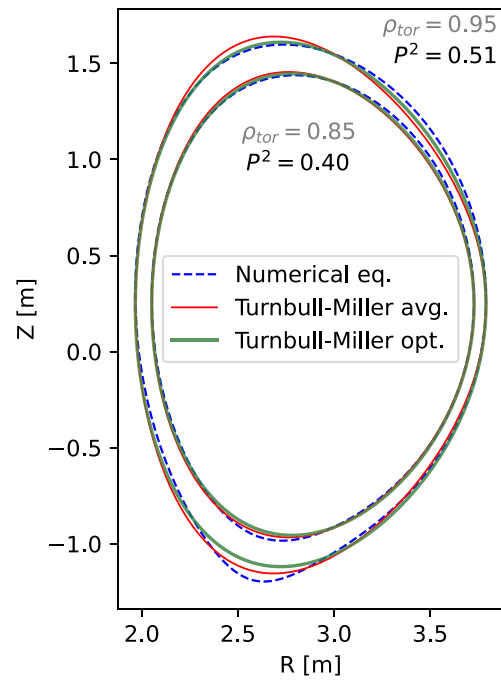
over a window of 200 ms during the L-mode phase of the discharges. For #83164 (15.05–15.25 s), $\rho_{\text{inv}} \approx 0.380$, while for #95473 (12.7–12.9 s), $\rho_{\text{inv}} \approx 0.319$. An ESCO grid of 451×451 points was required to ensure accurate safety factor and magnetic shear profiles near the boundary.

Flux-surfaces at $\rho_{\text{tor}} = 0.85$ and $\rho_{\text{tor}} = 0.95$ were traced on the two-dimensional poloidal flux maps output by ESCO for both discharges, see the blue dashed lines in Fig. 1. Averaged analytic and optimized fit Turnbull–Miller parameterizations, as shown in Fig. 1 with thin red and thicker green lines, respectively, were computed with MEGPy using the routine described in Sec. III. The optimized fit parameterizations fit the numerical flux-surface contours better, in particular on the low-field side (right half) and on the top. Contour-averaged absolute errors in ℓ_1 and ℓ_2 for the optimized fits were on average $\sim 1.3\times$ smaller than those of the analytical parameterizations for the cases shown in Fig. 1. The optimization achieved this mainly by finding better fitting values for elongation, triangularity, and squareness.

To further quantify fit quality, we show P^2 , which replaces the total sum of squares in the denominator of the coefficient of determination R^2 with the residual sum of squares of the averaged analytical parameterization. See Appendix B for more details on P^2 . Positive values for P^2 mean that the optimized fit is that fraction better than the averaged analytical approximation, with $P^2 = 1$ for a perfect fit, while negative values indicate that the optimized fit is worse. For all the examples in Fig. 1, $P^2 > 0$, with significantly smaller average residuals



(a)



(b)

FIG. 1. Flux-surfaces at $\rho_{\text{tor}} = 0.85$ (inner) and $\rho_{\text{tor}} = 0.95$ (outer) for JET-ILW discharges (a) #83164 and (b) #95473, with the exact numerical equilibrium from ESCO (blue dash) and the averaged analytic (red) and optimized fit (green) Turnbull–Miller parameterizations, respectively. (a) JET-ILW #83164 (15.05–15.25 s). (b) JET-ILW #95473 (12.7–12.9 s).

for the optimized fits when compared to the averaged analytical parameterizations.

Remaining discrepancies in the lower-left quadrant between the numerical and optimized parameterizations are due to the inherent up-down symmetry limitations of the Turnbull-Miller formulation. Overall, it is clear that the optimization routine is capable of fitting more accurate flux-surface contours.

To be able to take reliable derivatives of the shape parameters and compute the parameterized poloidal magnetic field B_p , smooth radial profiles are required. Looking at examples for JET-ILW #83164 in Figs. 2 and 3, the optimization routine also succeeded at this. Radial profiles of the optimized shape parameters are smooth; thus, the routine does not appear prone to local overfitting. Significant differences between the averaged analytical and optimized elongation, triangularity, and squareness start appearing past $\rho_{tor} = 0.75$. As a result, the optimized poloidal magnetic field parameterizations are also significantly more accurate, see, e.g., Fig. 3 for B_p for JET-ILW #83164 at $\rho_{tor} = 0.95$, especially on the low-field side. Furthermore, the relative error Δ of the contour-average of the overall magnetic field is also always significantly smaller for the optimized than the averaged analytical parameterizations, as, e.g., for JET-ILW #83164 can be seen in Fig. 4. Toward the LCFS, it levels off due to increased average error in B_t balancing against reduced error in B_p .

For numerical convergence of the obtained shape parameters, the typical amount of points in the numerical reference flux-surface traces for our equilibria ($N_\theta \approx 1500$) seemed sufficient. When up-sampling

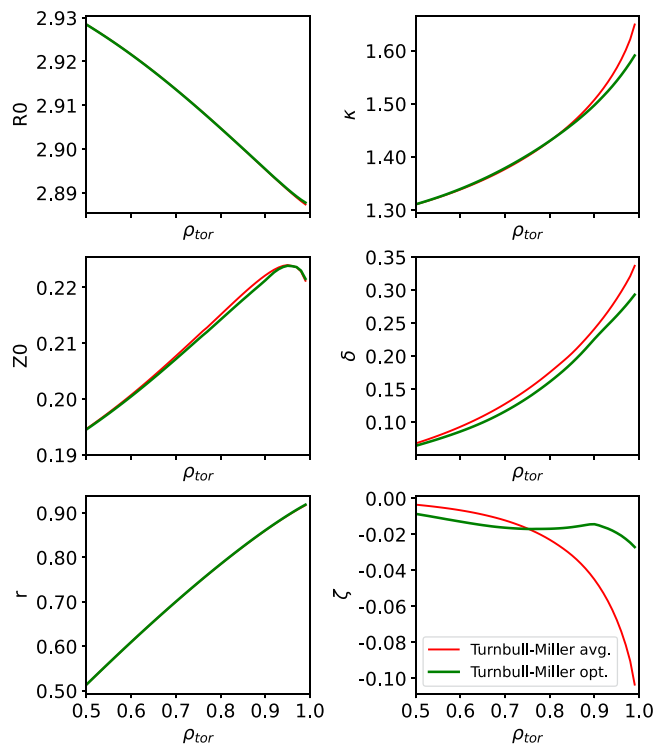


FIG. 2. Radial profiles for JET-ILW discharge #83164 of the shape parameters R_0 , κ , Z_0 , δ , r , ζ (from left to right, top to bottom) for $\rho_{tor} \in [0.5, 1.0]$, with the averaged analytic values in red and the optimized fit values in green.

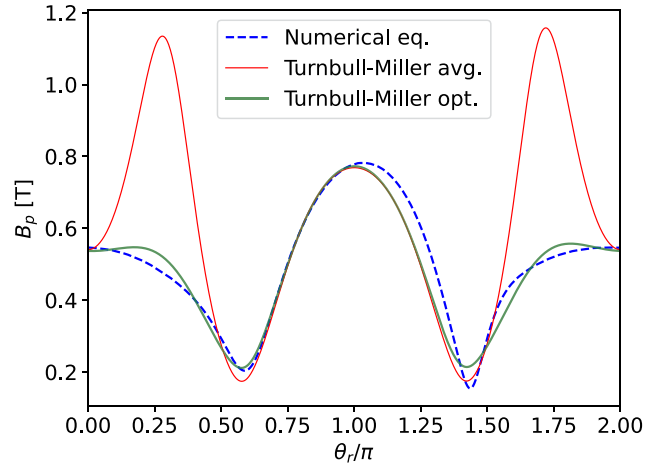


FIG. 3. Poloidal magnetic field as a function of θ_r for JET-ILW discharge #83164 at $\rho_{tor} = 0.95$, with the exact numerical equilibrium (blue dash) and the averaged analytical (red) and optimized (green) parameterizations. $\theta_r = 0, 2\pi$ are on the out-board side.

the number of poloidal points of the reference contours for our cases up to $N_\theta = 7200$ through interpolation, the only parameters that changed noticeably were the triangularity (<1%) and squareness (<5%) and their derivatives, with the other parameters being constant. Moreover, these minor value changes had a negligible impact on the contour-average relative errors of both the flux-surface contour and B_p ; thus, typically no up-sampling should be required.

The `scipy` implementation of the TIR algorithm used to solve the least squares converges rapidly and seems to scale $\mathcal{O}(\sqrt{n})$. Increasing the number of poloidal points N_θ included in the least squares $10\times$ increased the average computational time of the optimization routine per flux-surface by less than $3\times$, while the number of function evaluations required per parameterization optimization

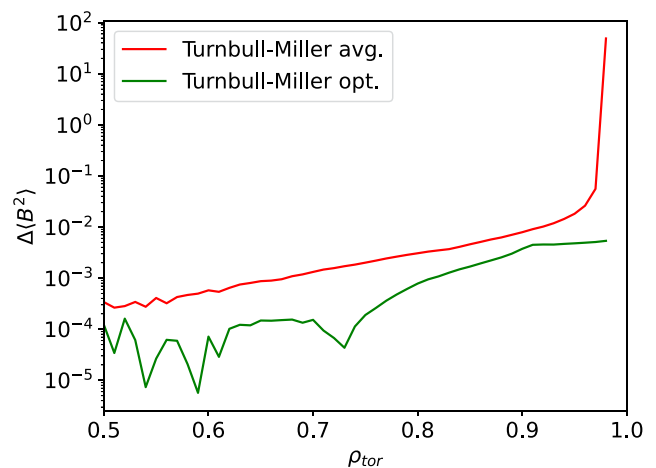


FIG. 4. Relative error Δ of contour-average B^2 as a function of $\rho_{tor} \in [0.5, 1.0]$ for JET-ILW discharge #83164, with red and green the averaged analytical and optimized parameterizations, respectively.

varied by less than ten percent. Even at $N_\theta = 7200$, the average computational time of the optimization routine per flux-surface was only less than one second wall time, which is about two orders of magnitude larger than for the analytical calculations.

In addition to the TIR algorithm, the commonly used Levenberg–Marquardt algorithm²⁹ with a linear residual function $\rho(s) = s$ was also considered. However, this performed worse when compared in the final cost (at least two orders of magnitude higher), fit to the reference flux-surface contour (10–20% larger contour-average absolute errors), and poloidal magnetic field error (~50% larger contour-average absolute errors).

V. IMPACT ON TURBULENCE SIMULATIONS

Linear, local gyrokinetic simulations of plasma microturbulence were performed with the GENE code¹⁷ to investigate the impact of the optimized parameterizations of the local equilibrium. Plasma parameters and equilibria from the two JET-ILW discharges (#83164 and #95473) at the two radial locations used in Sec. IV ($\rho_{\text{tor}} = 0.85$ and $\rho_{\text{tor}} = 0.95$) were used, see Table I for (optimized) input values. Per radial location simulations were performed with three equilibria: (1) a numerical equilibrium from ESCO (mapped onto the GENE grid by TRACER); (2) the averaged analytical parameterization; and (3) the optimized fit parameterization.

Initial value simulations were setup with two kinetic species, electrons and deuterium ions, with a Landau collision operator. Electromagnetic effects, including parallel magnetic fluctuations, were switched on. Plasma rotation was not included in the simulations. GENE uses field-aligned coordinates $\{x, y, z, v_{\parallel}, \mu\}$, where x and z are the radial and field-aligned coordinates, respectively, y is the binormal coordinate, i.e., orthogonal to both x and z , v_{\parallel} is the parallel velocity, and μ is the magnetic moment. At $\rho_{\text{tor}} = 0.85$, $[n_x, n_z, n_{v_{\parallel}}, n_{\mu}] = [17, 48, 64, 18]$ were used as numerical resolutions, while at $\rho_{\text{tor}} = 0.95$, $[n_x, n_z, n_{v_{\parallel}}, n_{\mu}] = [17, 128, 64, 18]$ were used.

In simulations with the ESCO numerical equilibria, 14 binormal wavenumbers $k_y \in [0.1, 2.0]$ were used, while in simulations with parameterized local equilibria, the corresponding toroidal mode numbers n_{tor} were used to allow direct comparison of the linear spectra. Hyperdiffusion along the z -direction was set to $h_z = 5$.

The linear initial value simulations only output the growth rate and frequency of the fastest growing mode for each wavenumber. In Fig. 5, the linear spectra for the two JET-ILW discharges at the two different radii are presented, and in blue squares, red triangles, and green dots, the results from the simulations with numerical equilibria, averaged analytical, and optimized parameterizations are presented, respectively. In the GENE convention, negative frequencies indicate modes in the electron diamagnetic drift direction, while positive frequencies correspond to modes in the ion diamagnetic drift direction, as indicated in the figures. Matching the linear growth rate spectra from the simulations using numerical equilibria indicates that the turbulence drives are predicted correctly. This is especially important for instabilities in the low mode number/wavenumber range, where the characteristic length scales of the turbulence are on the order of ion gyroradii and most of the transport is generated. Furthermore, getting the linear spectra correct is also important for accurate predictions by quasi-linear turbulent transport models, such as TGLF.

The linear spectra for both #83164 and #95473 at $\rho_{\text{tor}} = 0.85$ show a relative close match for both the averaged analytical and

optimized fit parameterized equilibria, although the P^2 values for the flux-surface contours indicated that the optimized fits were significantly closer to the numerical equilibria. The dominant linear mode in #83164 is a hybrid mode,³⁰ based on the frequency spectrum and cross-phases between electrostatic potential and density and temperature fluctuations (not shown here), while #95473 is dominated by trapped electron modes (TEM). The root mean square error (RMSE) for the linear growth rates with the optimized parameterizations is about half those with the averaged analytical for #83164 and about twice those for #95364. The linear frequencies are also matched better by optimized fit for #83164, while for #95473, the absolute errors are about the same.

For the linear spectra at $\rho_{\text{tor}} = 0.95$, the differences are larger. Both discharges have similar dominant linear modes, again hybrid modes based on the frequency spectra and mode cross-phases (not shown). For #83164 at this radius, there is a minor improvement in the linear growth rate RMSE. Although the low mode number ion-scale modes are significantly more accurately captured with the optimized parameterization, the errors for the smaller scale modes remain similar to those with averaged analytical parameterization. The trend in the frequencies is also more accurately reflected in the optimized parameterization simulations. The differences for #95473 at $\rho_{\text{tor}} = 0.95$ are more notable. In this case, the averaged analytical parameterizations are significantly under-predicting the linear growth rates in the low mode number range, with a RMSE more than three times as big as for the optimized fit. The simulation with the optimized parameterization approximates the one with the numerical equilibrium closely for both the linear growth rate and frequency spectra, as well as getting the transition in ballooning representation of the modes (not shown here) correct as well. Although $P^2 > 0.5$ for both discharges, higher P^2 values do not correlate directly with more accurate linear gyrokinetic results. In addition to the flux-surface geometry, the local equilibrium parameterization affects i.a. magnetic resonances and all the gradient operators in the gyrokinetic equations, which P^2 does not quantify.

VI. ASYMMETRIC PARAMETERIZATIONS

To demonstrate that the presented method generalizes to any analytical local equilibrium parameterization, we repeat the previous linear gyrokinetics validation step for both JET-ILW cases at $\rho_{\text{tor}} = 0.95$ now with the aforementioned Fourier expansion (as implemented in GENE) and MXH parameterizations. For convenience, both are briefly summarized and any differences compared to Turnbull–Miller with respect to the optimization routine as listed in Sec. III are highlighted.

The general Fourier expansion⁶ as implemented in the GENE code, called `miller_general`, is given by³¹

$$\begin{aligned} R_s &= R_0 + r_{\text{shape}}(\theta, r) \cos(\theta), \\ Z_s &= Z_0 + r_{\text{shape}}(\theta, r) \sin(\theta), \end{aligned} \quad (18)$$

where

$$r_{\text{shape}} \doteq \sum_{n=0}^{N-1} [c_n(r) \cos n\theta + s_n(r) \sin n\theta]. \quad (19)$$

The MXH flux-surface parameterization⁸ is given by

$$\begin{aligned} R_s &= R_0(r) + r \cos(\theta_R(\theta, r)), \\ Z_s &= Z_0(r) + r \kappa \sin(\theta), \end{aligned} \quad (20)$$

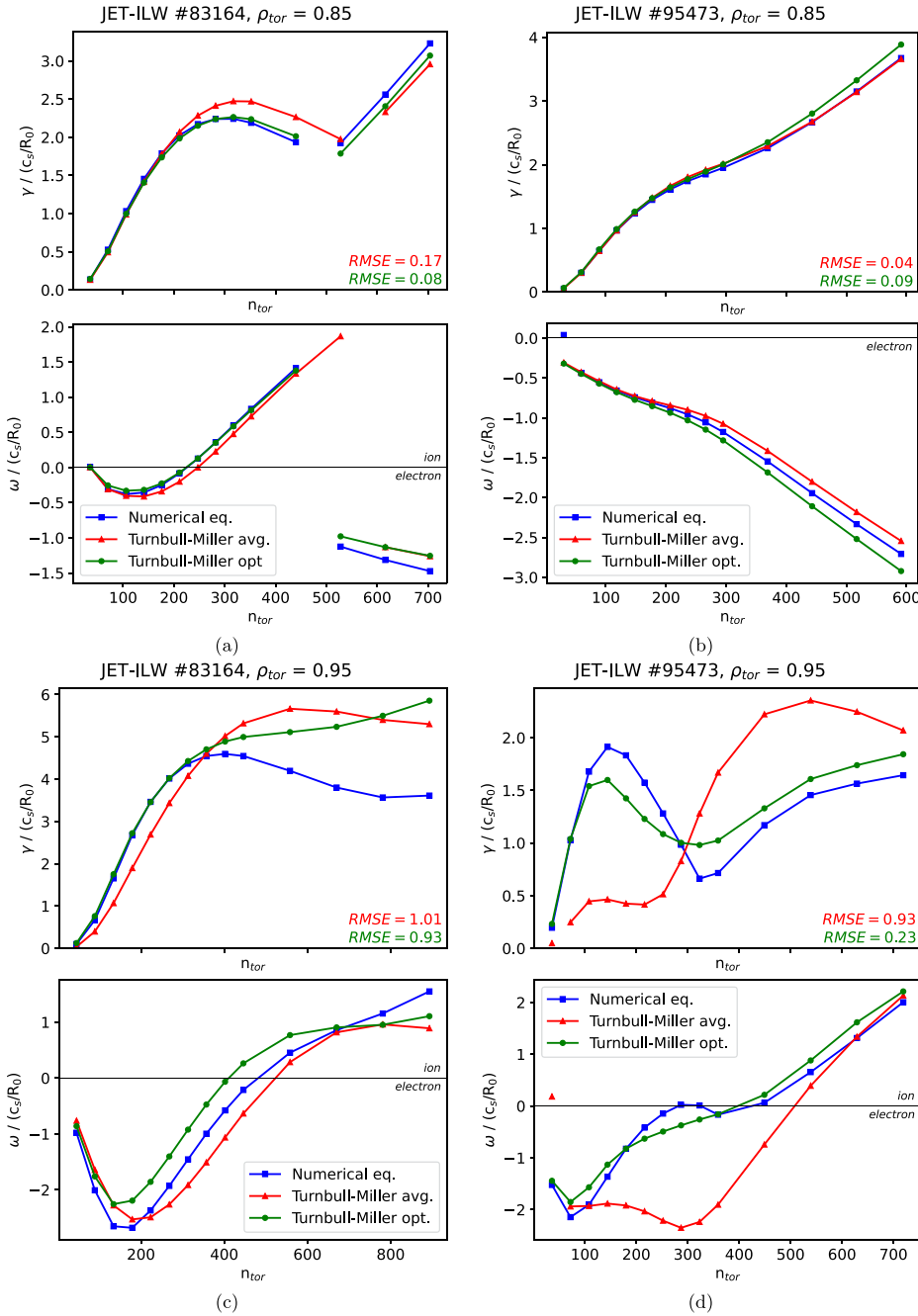


FIG. 5. The normalized linear growth rate $\gamma / (c_s/R_0)$ (top) and frequency $\omega / (c_s/R_0)$ (bottom) of the most unstable modes as a function of toroidal mode number n_{tor} . The results from local gyrokinetic simulations with GENE for JET-ILW discharges #83164 [(a) and (c)] and #95473 [(b) and (d)] at two radial locations each ($\rho_{tor} = 0.85$, $\rho_{tor} = 0.95$) for two different approaches of calculating the shape parameters for the local Turnbull-Miller parameterization (red triangles and green circles) are compared with simulations using their respective numerical equilibrium solution (blue squares).

08 August 2023 09:48:08

where

$$\theta_R \doteq \theta + c_0(r) + \sum_{n=1}^N [c_n(r) \cos n\theta + s_n(r) \sin n\theta]. \quad (21)$$

For both generalized parameterizations, the plasma major and minor radii R_0 and r , average elevation Z_0 , and elongation κ (in the case of MXH) are calculated from a bounding box on the flux-surface

contour. Given that s_0 drops out in the general Fourier case and is not included in MXH, both parameterizations effectively require a similar set of shape parameters to be solved,

$$\mathbf{x} = \{c_0, c_1, s_1, \dots, c_n, s_n\}. \quad (22)$$

Thus, a total of $n_{shape} = 2 + 2N$ shape parameters is required for the Fourier expansion of the flux-surface, while MXH requires

$n_{\text{shape}} = 5 + 2N$ shape parameters, of which $1 + 2N$ are fitted for both parameterizations. Although tempting, including R_0 , Z_0 , r , and κ in the optimization of \mathbf{x} tends to result in non-smooth profiles for the other shaping parameters, this is, therefore, not recommended.

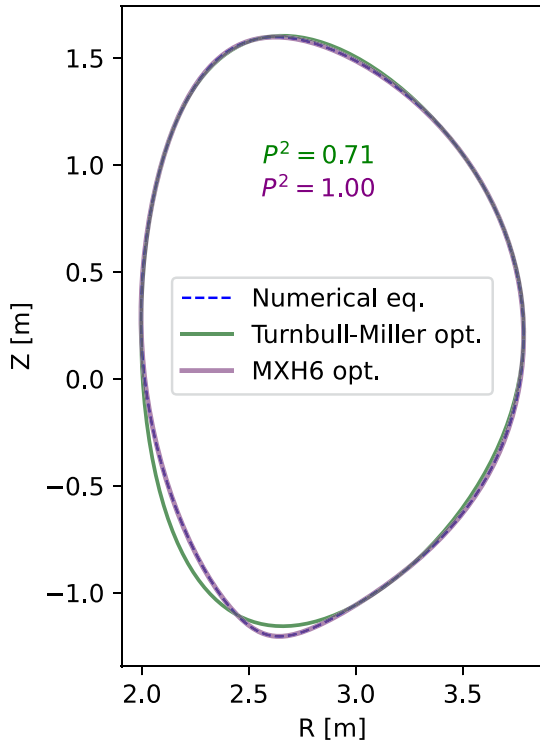
The two parameterizations differ in their sets of shape derivative parameters, given by

$$\hat{\mathbf{x}}_{\text{Fourier}} = \{\partial_r c_0, \partial_r c_1, \partial_r s_1, \dots, \partial_r c_n, \partial_r s_n\} \quad (23)$$

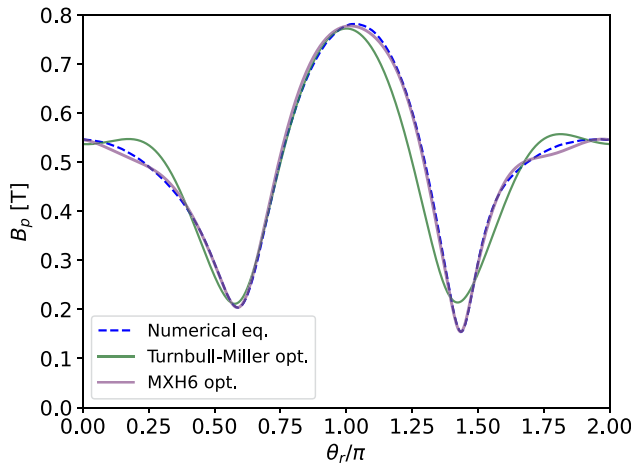
and

$$\hat{\mathbf{x}}_{\text{MXH}} = \{\partial_r R_0, \partial_r Z_0, s_{\kappa}, s_{c_0}, s_{c_1}, s_{s_1}, \dots, s_{c_n}, s_{s_n}\}, \quad (24)$$

where the normalized shape derivatives s_{c_0} are of the same form as s_{ζ} in Eq. (11). The Fourier implementation in GENE has a fixed plasma major radius and elevation for every flux-surface, hence the absence of $\partial_r R_0$ and $\partial_r Z_0$.

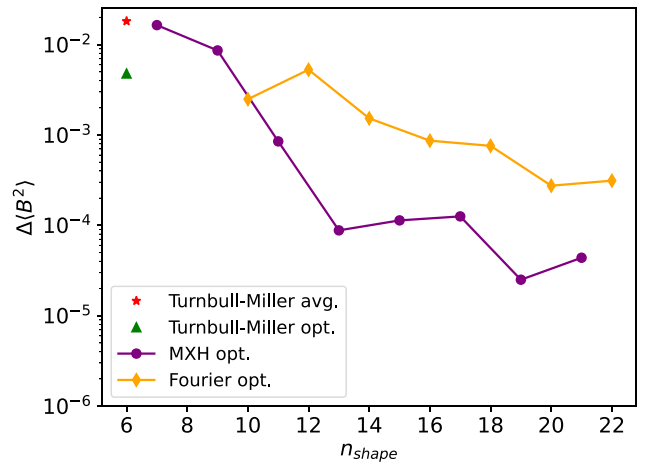


(a)

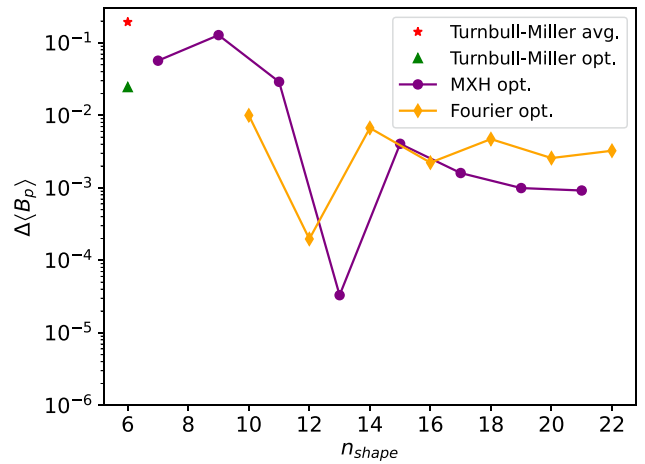


(b)

FIG. 6. Flux-surfaces (a) and B_p (b) for $\rho_{\text{tor}} = 0.95$ JET-ILW #83164 (15.05–15.25 s), with the exact numerical equilibrium solution from ESCO (blue dash) and Turnbull-Miller (green) and MXH6 (purple) parameterizations, respectively, both calculated with our optimization routine. (a) JET-ILW #83164 flux-surface at $\rho_{\text{tor}} = 0.95$. (b) JET-ILW #83164 B_p at $\rho_{\text{tor}} = 0.95$.



(a)



(b)

FIG. 7. Relative errors Δ for (a) contour-average total magnetic field squared (B^2) and (b) contour-average poloidal magnetic field (B_p) as a function of the number of shape parameters n_{shape} included in the contour parameterization for JET-ILW #83164 at $\rho_{\text{tor}} = 0.95$. Data shown for averaged analytic Turnbull-Miller (red star, $n_{\text{shape}} = 6$), optimized Turnbull-Miller (green triangle, $n_{\text{shape}} = 6$), MXH (purple circles, $n_{\text{shape}} = 5 + 2N$), and general Fourier (orange diamonds, $n_{\text{shape}} = 2 + 2N$) parameterizations. (a) $\Delta(B^2)$ (b) $\Delta(B_p)$.

08 August 2023 09:48:08

As initial condition, all shape parameters are set to zero for MXH and linearly decreasing between one and zero for the Fourier expansion [or the result of a truncated fast Fourier transform (FFT) can be used]. For MXH, all the shaping is implemented as phase modifications to the radial flux-surface coordinate only; thus, there the θ -grid can be calculated directly from the discrete reference flux-surface vertical coordinates and no re-basing on θ_s is required. Despite these differences compared with Turnbull–Miller and the larger set of shape parameters to solve, the optimization routine described in Sec. III retains similar performance without the need for modifications.

The generalized parameterizations have significantly more shaping parameters than Turnbull–Miller ($n_{\text{shape}} = 6$). This increases the versatility of such general parameterizations to match complex flux-surface shapes. See, for example, Fig. 6 where MXH6 ($N = 6$), which considered a proxy for the exact solution by Arbon *et al.*,⁸ is compared against the optimized Turnbull–Miller result and the numerical equilibrium solution for JET-ILW #83164 at $\rho_{\text{tor}} = 0.95$. In contrast to the optimized Turnbull–Miller solution $P^2 = 1$, although some minor discrepancies in B_p remain. Two more such examples for numerical equilibria with more complex shaping (tilting and complex asymmetry) are shown in Figs. 9 and 10, Appendix C.

While the number of shape parameters is of similar order, the accuracy of the MXH parameterization converges much faster with the number of parameters than the general Fourier expansion, as already highlighted by Arbon *et al.* As an example of this, see Fig. 7, where the relative contour-average errors in the total magnetic field (B^2) and poloidal magnetic field component (B_p) compared with the numerical equilibrium solution for JET-ILW #83164 at $\rho_{\text{tor}} = 0.95$ are shown for all of the parameterizations considered in this work. Increasing the number of included harmonics in MXH ($N = 1, 2, 3, \dots$) decreases the errors in the magnetic field rapidly and significantly, while for the general Fourier expansion this reduction is much

smaller. It is important to note though that even while contour-average errors in the poloidal magnetic field can be of similar order of magnitude, visual inspection of the poloidal profiles showed that for a similar amount of shape parameters the MXH profiles were significantly closer to the numerical equilibrium solution.

The linear gyrokinetic simulations performed with the Turnbull–Miller parameterizations at ρ_{tor} of JET-ILW discharges #83164 and #95473 were repeated for both the Fourier and MXH parameterizations. For this, the MXH parameterization was added to the GENE code. The same GENE settings as for the Turnbull–Miller parameterizations were used, see Fig. 8 for the results. Initial simulations were performed with MXH6 (not shown here), given the results by Arbon *et al.* However, it was found that a significant improvement for a few hard to match toroidal mode numbers could be achieved by doubling the amount of shape parameters (MXH12) in the #95473 case. No such further improvement was seen in the #83164 case. For comparison, simulations with the maximum number of shape parameters possible in GENE for the Fourier parameterization ($N = 32$) were performed. As expected, overall the linear growth rate and frequency spectra of simulations with both generalized parameterizations are significantly closer to those from simulations with the numerical equilibria than those for the optimized Turnbull–Miller parameterizations. The optimized Fourier parameterization simulations were also compared against ones with shape coefficients determined by truncated fast Fourier transform (not shown) and found to match the numerical equilibrium solutions similarly or marginally better. Remaining differences between the linear spectra from simulations with local parameterization and simulations with the numerical equilibria are most likely due to: (1) numerical differences caused by mapping and tracing of the rasterized numerical equilibrium input into GENE; (2) the two geometry options using different radial coordinates, ρ_{tor} in simulations with the numerical equilibrium vs r in

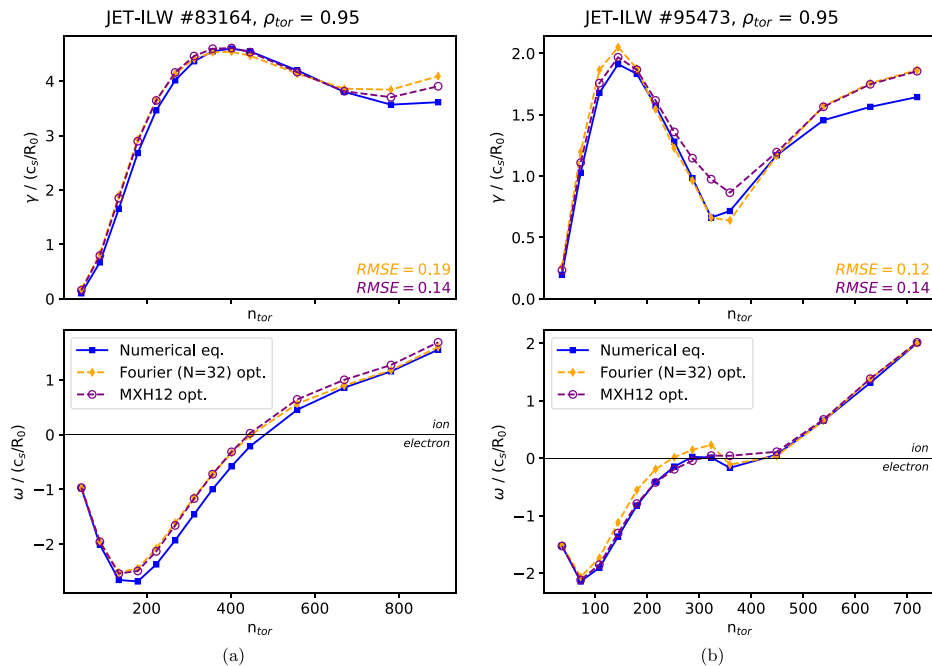


FIG. 8. The normalized linear growth rate $\gamma / (c_s/R_0)$ (top) and frequency $\omega / (c_s/R_0)$ (bottom) of the most unstable modes as a function of toroidal mode number n_{tor} . The results from local gyrokinetic simulations with GENE for JET-ILW discharges #83164 (a) and #95473 (b) at $\rho_{\text{tor}} = 0.95$ are compared for two optimized parameterizations, Fourier (orange diamonds) and MXH12 (purple circles), with simulations using their respective numerical equilibrium solution (blue squares).

simulations with parameterized geometry, which can lead to further mapping differences (e.g., increasing the magnetic shear for #95473 at $\rho_{\text{tor}} = 0.95$ by less than 5% further reduces some of the discrepancies); or (3) the locally linearized approximation of the numerical equilibrium might not hold exactly this close to the last-closed flux-surface.

VII. CONCLUSIONS AND DISCUSSION

We have developed a fast and accurate method of determining shape parameters that best fit a reference flux-surface for a given analytic flux-surface parameterization. The optimization routine was demonstrated to result in significantly more accurate parameterizations of the local magnetohydrodynamic equilibrium for the popular Turnbull–Miller formulation. Flux-surface contour-average errors for optimized fits were found to be up to thirty percent smaller than those of the traditional averaged analytical parameterizations. Radial profiles of optimized shape parameters were found to be smooth, with no signs of overfitting. Their radial derivatives resulted in significantly more accurate parameterizations of the poloidal magnetic field component along the flux-surface contours, especially on the low-field side of the plasma. Relative errors of the contour-averaged parameterized magnetic field were found to always be smaller than those for traditional analytical parameterizations.

The optimization routine scales $\mathcal{O}(\sqrt{n})$ with the number of poloidal points and converges within less than one second wall time. Although two orders of magnitude slower than traditional analytic calculations, this is an upper limit as typical numerical equilibria do not include as many grid points as used in this work. This is fast enough to be useful for integrated transport modeling of the full plasma volume inside the last-closed flux-surface, especially if parallelized or only applied for radii $\rho_{\text{tor}} \geq 0.75$.

We have shown that, although Turnbull–Miller only allows for up-down symmetric flux-surface contours, modest up-down asymmetry near the plasma boundary does not appear to prevent its use with optimized fits. Local, linear gyrokinetic simulations of the plasma microturbulence for two JET-ILW discharges showed that optimized parameterizations of their local equilibria resulted in more accurate linear growth rate and frequency spectra, particularly at the crucial ion-scale, where most transport due to turbulence originates, and most notably in more strongly shaped regions of the plasma.

Thus, our method extends the usability of the Turnbull–Miller parameterization, while it can also easily be utilized for generalizations thereof.

ACKNOWLEDGMENTS

The authors are grateful to Timo Ravensbergen for an interesting discussion on cost functions for nonlinear least squares and to Aaron Ho for his insight into the metrics of goodness. We would like to thank Yann Camenen for providing several numerical equilibria with strong asymmetry.

This work has been carried out within the framework of the EUROfusion Consortium, funded by the European Union via the Euratom Research and Training Programme (Grant Agreement No. 101052200—EUROfusion). Views and opinions expressed are, however, those of the author(s) only and do not necessarily reflect those of the European Union or the European Commission. Neither the European Union nor the European Commission can be held responsible for them.

DIFFER is a part of the institutes organization of NWO.

AUTHOR DECLARATIONS

Conflict of Interest

The authors have no conflicts to disclose.

Author Contributions

Garud Snoep: Conceptualization (equal); Data curation (equal); Formal analysis (lead); Methodology (lead); Software (lead); Validation (lead); Visualization (lead); Writing – original draft (lead); Writing – review & editing (equal). **Jesse Koenders:** Conceptualization (equal); Formal analysis (supporting); Methodology (supporting); Validation (supporting); Writing – original draft (supporting); Writing – review & editing (equal). **Clarisse Bourdelle:** Conceptualization (supporting); Funding acquisition (equal); Resources (equal); Supervision (equal); Writing – original draft (supporting); Writing – review & editing (equal). **Jonathan Citrin:** Conceptualization (supporting); Funding acquisition (equal); Resources (equal); Supervision (equal); Writing – original draft (supporting); Writing – review & editing (equal).

DATA AVAILABILITY

The data that support the findings of this study are available upon reasonable request from the corresponding author. The Python code used to perform the parameterizations in this work is freely available on GitHub.²³

APPENDIX A: METHODS FOR OPTIMIZATION OF SHAPE DERIVATIVE QUANTITIES

If one considers the set of shape derivative quantities as more degrees of freedom to be optimized, there are two possible approaches: (1) solve the union of \mathbf{x} and $\hat{\mathbf{x}}$ with a single optimization routine or (2) first solve \mathbf{x} using the optimization routine from Sec. III and subsequently solve $\hat{\mathbf{x}}$ with an additional minimization problem. As all these options were explored over the course of this work, but ultimately not used, we list them here for completeness.

Although the all-at-once option seems ideal, as it should prevent solving the parameterization of the local equilibrium for a local minimum of the contour fit, it was found to be a challenging optimization problem to implement in practice. Nevertheless, the following are three possible approaches to this:

- Extend the optimization routine presented in Sec. III by adding the ℓ_1 distance for B_p to the residual f_i . This simultaneously penalizes errors in the parameterization of the flux-surface contour and poloidal magnetic field. Unfortunately, we found this approach not tractable with the least squares solvers used in this work, as the algorithms ran out of function evaluations before reaching the residual thresholds (even when raised orders of magnitude).
- Replace the ℓ_1 and ℓ_2 distances for the flux-surface contour with the ℓ_1 distance for B_p in the residual f_i , as Eq. (4) includes both the shape and shape derivative parameters. Although this can result in small errors in the parameterized B_p , for the cases considered in this work the solver achieved this by forcing shape parameters inconsistent with the reference flux-surface contour and it required narrow bounds to get reasonable results. Thus, this results in an underconstrained problem, and narrow,

case-specific bounds defeat the purpose of a generalized fitting algorithm.

- Extend the optimization routine in Sec. III by adding the ℓ_1 distances for $\partial_r R_s$, $\partial_r Z_s$, $\partial_\theta R_s$ and $\partial_\theta Z_s$ to the residual f_i . However, for the Turnbull-Miller parameterization, this is challenging to implement as it requires knowing r and the θ_s -grid for multiple flux-surfaces in order to be able to calculate radial and poloidal derivatives of the reference flux-surface contour at the radial position of interest. Nested loops of optimization are then unavoidable, which increases the complexity and thus slows down the routine.

The two-stage optimization option turned out to be more practical. Two possible approaches were implemented in MEGPy, which are as follows:

- Solve \hat{x} by minimizing the ℓ_1 distance for B_p for the radial position of interest. This produces shape-derivative parameters that generally provide a smaller error in the poloidal magnetic field parameterization than calculating them self-consistently from radial profiles of the shape parameters, especially on the low-field side. However, the resulting parameterizations can be inconsistent with the (numerically generated) Grad-Shafranov equilibrium solution as minimizing the error in B_p means effectively minimizing the error in the sum of gradient terms in the Jacobian of the parameterization. Therefore, when performing linear gyrokinetic simulations with these parameterizations, the benefits of the lower error in the poloidal magnetic field can be negated by the increased errors in the radial derivatives of the flux-surface shape that cascade through the gradient operators in the physics equations solved. Thus, we found that sometimes it can be beneficial, but it is unpredictable beforehand.
- Solve \hat{x} by minimizing the ℓ_1 distances for $\partial_r R_s$, $\partial_r Z_s$, $\partial_\theta R_s$ and $\partial_\theta Z_s$ for the radial position of interest. This guarantees a parameterization consistent with the numerically generated Grad-Shafranov solution. Nevertheless, the resulting shape-derivative values were very close to the values calculated from fitting multiple, closely spaced flux-surface contours and taking the radial derivatives (the “self-consistent” option from Sec. III). Often, the contour-average error in the poloidal magnetic field was actually higher. As a result, the linear gyrokinetic spectra were also very close to the simulations with self-consistent \hat{x} (<5% difference).

Thus, although it might seem tempting to consider the shape-derivative parameters as additional degrees of freedom to be optimized, in practice computing the radial derivatives for multiple closely spaced flux-surfaces self-consistently generally results in the most accurate linear gyrokinetic spectra and is, therefore, the recommended approach.

APPENDIX B: QUANTIFYING FIT ACCURACY

To quantify the quality of an optimized fit to a reference flux-surface contour, we replace the total sum of squares SS_{tot} in the denominator of the coefficient of determination R^2 with the residual sum of squares of the averaged analytical parameterization,

$$p^2 = 1 - \frac{SS_{res,o}}{SS_{res,a}}, \tag{B1}$$

where the indices o and a indicate the optimized fit and averaged analytical parameterizations, respectively,

$$SS_{res,o} = \sum_i \left(\sqrt{R_{r,i}^2 + Z_{r,i}^2} - \sqrt{R_{o,i}^2 + Z_{o,i}^2} \right)^2, \tag{B2}$$

$$SS_{res,a} = \sum_i \left(\sqrt{R_{r,i}^2 + Z_{r,i}^2} - \sqrt{R_{a,i}^2 + Z_{a,i}^2} \right)^2, \tag{B3}$$

where the index r indicates the numerical reference flux-surface, and i is the index of the poloidal sample. This is a more meaningful metric than R^2 , as that effectively compares the parameterizations against a circle with the average minor radius of the reference flux-surface contour and thus always leads to $R^2 \approx 1$.

APPENDIX C: EXAMPLES OF COMPLEX SHAPING

The optimization routine has no problem handling complex shaping (tilting, asymmetry, etc.). See two more examples of flux-surfaces at $\rho_{tor} = 0.95$ traced on numerical Grad-Shafranov equilibrium solutions generated with the CHEASE code³² in Figs. 9 and 10.

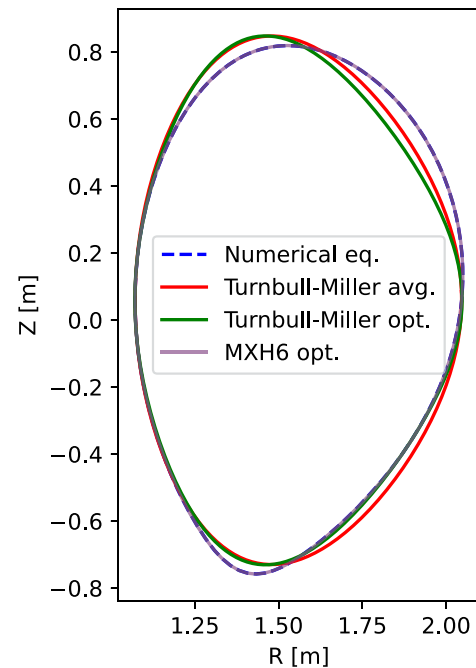


FIG. 9. Shaped and tilted flux-surface at $\rho_{tor} = 0.95$, with the averaged analytical Turnbull-Miller parameterization (red) and the optimized Turnbull-Miller (green) and MXH6 (purple) parameterizations, respectively, compared against the exact numerical equilibrium solution from CHEASE (blue dash).

08 August 2023 09:48:08

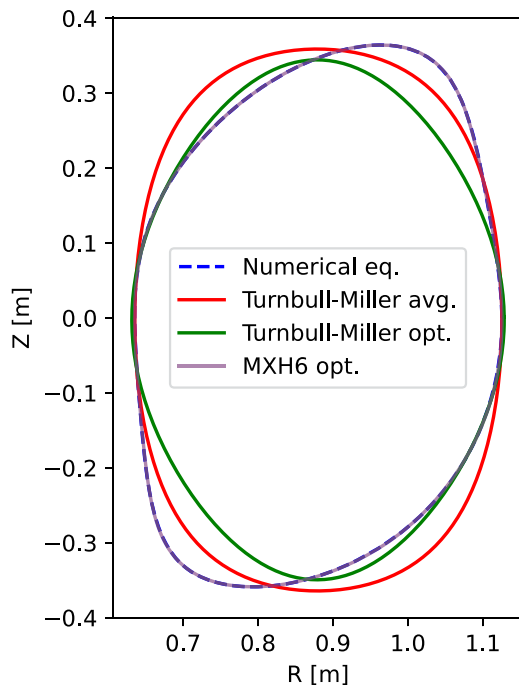


FIG. 10. Complex asymmetrical flux-surface at $\rho_{\text{tor}} = 0.95$, with the averaged analytical Turnbull-Miller parameterization (red) and the optimized Turnbull-Miller (green) and MXH6 (purple) parameterizations, respectively, compared against the exact numerical equilibrium solution from CHEASE (blue dash).

REFERENCES

- ¹C. Mercier and H. Luc, Report No. EUR-5127e 140 (Commission of the European Communities, Brussels, 1974).
- ²R. L. Miller, M. S. Chu, J. M. Greene, Y. R. Lin-Liu, and R. E. Waltz, "Noncircular, finite aspect ratio, local equilibrium model," *Phys. Plasmas* **5**, 973–978 (1998).
- ³J. Greene and M. Chance, "The second region of stability against ballooning modes," *Nucl. Fusion* **21**, 453–464 (1981).
- ⁴C. Bishop, P. Kirby, J. Connor, R. Hastie, and J. Taylor, "Ideal MHD ballooning stability in the vicinity of a separatrix," *Nucl. Fusion* **24**, 1579–1584 (1984).
- ⁵A. D. Turnbull, Y. R. Lin-Liu, R. L. Miller, T. S. Taylor, and T. N. Todd, "Improved magnetohydrodynamic stability through optimization of higher order moments in cross-section shape of tokamaks," *Phys. Plasmas* **6**, 1113–1116 (1999).
- ⁶J. Candy, "A unified method for operator evaluation in local Grad-Shafranov plasma equilibria," *Plasma Phys. Controlled Fusion* **51**, 105009 (2009).
- ⁷T. C. Luce, "A simplified analytic form for generation of axisymmetric plasma boundaries," *Plasma Phys. Controlled Fusion* **59**, 042001 (2017).
- ⁸R. Arbon, J. Candy, and E. A. Belli, "Rapidly-convergent flux-surface shape parameterization," *Plasma Phys. Controlled Fusion* **63**, 012001 (2021).
- ⁹R. Bravenec, J. Citrin, J. Candy, P. Mantica, and T. Görler, "Benchmarking the GENE and GYRO codes through the relative roles of electromagnetic and EXB stabilization in JET high-performance discharges," *Plasma Phys. Controlled Fusion* **58**, 125018 (2016).
- ¹⁰G. Merlo, O. Sauter, S. Brunner, A. Burckel, Y. Camenen, F. J. Casson, W. Dorland, E. Fable, T. Görler, F. Jenko, A. G. Peeters, D. Told, and L. Villard, "Linear multispecies gyrokinetic flux tube benchmarks in shaped tokamak plasmas," *Phys. Plasmas* **23**, 032104 (2016).

- ¹¹G. Staebler, E. A. Belli, J. Candy, J. Kinsey, H. Dudding, and B. Patel, "Verification of a quasi-linear model for gyrokinetic turbulent transport," *Nucl. Fusion* **61**, 116007 (2021).
- ¹²See https://sharepoint.iter.org/departments/POP/CM/IMDesign/Data%20Model/CI/imas-3.37.0/html_documentation.html for "ITER IMAS data dictionary documentation," accessed November 2022, requires ITER access.
- ¹³G. M. Staebler, J. E. Kinsey, and R. E. Waltz, "A theory-based transport model with comprehensive physics," *Phys. Plasmas* **14**, 055909 (2007).
- ¹⁴G. M. Staebler and J. E. Kinsey, "Electron collisions in the trapped gyro-landau fluid transport model," *Phys. Plasmas* **17**, 122309 (2010).
- ¹⁵C. Kiefer, C. Angioni, G. Tardini, N. Bonanomi, B. Geiger, P. Mantica, T. Pütterich, E. Fable, and P. Schneider, "Validation of quasi-linear turbulent transport models against plasmas with dominant electron heating for the prediction of ITER PFPO-1 plasmas," *Nucl. Fusion* **61**, 066035 (2021).
- ¹⁶C. Angioni, N. Bonanomi, E. Fable, P. Schneider, G. Tardini, T. Luda, and G. Staebler, "The dependence of tokamak L-mode confinement on magnetic field and plasma size, from a magnetic field scan experiment at ASDEX upgrade to full-radius integrated modelling and fusion reactor predictions," *Nucl. Fusion* **63**, 056005 (2023).
- ¹⁷F. Jenko, W. Dorland, M. Kotschenreuther, and B. N. Rogers, "Electron temperature gradient driven turbulence," *Phys. Plasmas* **7**, 1904–1910 (2000).
- ¹⁸See https://docs.scipy.org/doc/scipy/reference/generated/scipy.optimize.least_squares.html for "scipy.optimize.least_squares v1.9.3," accessed November 2022.
- ¹⁹M. A. Branch, T. F. Coleman, and Y. Li, "A subspace, interior, and conjugate gradient method for large-scale bound-constrained minimization problems," *SIAM J. Sci. Comput.* **21**, 1–23 (1999).
- ²⁰B. Triggs, P. F. McLauchlan, R. I. Hartley, and A. W. Fitzgibbon, "Bundle Adjustment — A Modern Synthesis" in *Vision Algorithms: Theory and Practice, Lecture Notes in Computer Science* edited by B. Triggs, A. Zisserman, and R. Szeliski (Springer, Berlin, Heidelberg, 2000), pp. 298–372.
- ²¹P. J. Huber, "Robust estimation of a location parameter," *Ann. Math. Stat.* **35**, 73–101 (1964).
- ²²H. Zou and T. Hastie, "Regularization and variable selection via the elastic net," *J. R. Stat. Soc. Ser. B* **67**, 301–320 (2005).
- ²³See <https://www.github.com/gsnoep/megpy> for "MEGPy."
- ²⁴P. Vincenzi, E. R. Solano, E. Delabie, C. Bourdelle, G. Snoep, A. Baciero, G. Birkenmeier, P. Carvalho, M. Cavedon, M. Chernyshova, J. Citrin, J. M. Fontdecaba, J. C. Hillesheim, A. Huber, C. Maggi, S. Memmuir, and F. I. Parra, "Power balance analysis at the L-H transition in Jet-ILW NBI-heated deuterium plasmas," *Plasma Phys. Controlled Fusion* **64**, 124004 (2022).
- ²⁵G. Cenacchi and A. Taroni, "JETTO: A free-boundary plasma transport code," Technical report (ENEA, Italy, 1988).
- ²⁶L. Appel and I. Lupelli, "Equilibrium reconstruction in an iron core tokamak using a deterministic magnetisation model," *Comput. Phys. Commun.* **223**, 1–17 (2018).
- ²⁷G. Szepesi, L. Appel, E. de la Luna, L. Frassinetti, P. Gaudio, M. Gelfusa, S. Gerasimov, N. Hawkes, M. Sertoli, D. Terranova, and JET Contributors, "Advanced equilibrium reconstruction for JET with EFIT++," in *47th EPS Conference on Plasma Physics* (2021), p. 3.1037.
- ²⁸A. Ho, J. Citrin, F. Auriemma, C. Bourdelle, F. Casson, H.-T. Kim, P. Manas, G. Szepesi, and H. Weisen, "Application of Gaussian process regression to plasma turbulent transport model validation via integrated modelling," *Nucl. Fusion* **59**, 056007 (2019).
- ²⁹J. Moré, "The Levenberg-Marquardt algorithm: Implementation and theory," in *Numerical Analysis*, edited by G. A. Watson (Springer, Berlin, Heidelberg, 1978), pp. 105–116.
- ³⁰M. Kammerer, F. Merz, and F. Jenko, "Exceptional points in linear gyrokinetics," *Phys. Plasmas* **15**, 052102 (2008).
- ³¹See "3.2.7 The geometry namelist" in "The gyrokinetic plasma turbulence code GENE: User manual" for "miller_general."
- ³²H. Lütjens, A. Bondeson, and O. Sauter, "The CHEASE code for toroidal MHD equilibria," *Comput. Phys. Commun.* **97**, 219–260 (1996).